



A Colorimetric and Fluorescent Probe Based on Rhodamine B for Detection of Fe³⁺ and Cu²⁺ Ions

Liqiang Yan¹ · Ya Xie¹ · Jianping Li¹

Received: 1 May 2019 / Accepted: 10 September 2019 / Published online: 10 October 2019
© Springer Science+Business Media, LLC, part of Springer Nature 2019

Abstract

Development of optical probe for the detections of Fe³⁺ and Cu²⁺ is one of the most active and interesting research directions in analytical chemistry because of their vital roles in the environment protection and human health. Herein, a turn on optical rhodamine B-based probe (probe 1) with the significant changes in color and fluorescence has been prepared. The color of this probe solution changed from colorless to amaranth in the presence of Fe³⁺ and to pink in the presence of Cu²⁺, which is promising for the qualitative recognition of Fe³⁺ and Cu²⁺. More importantly, probe 1 could be used for the quantitative analysis of Fe³⁺ and Cu²⁺ by fluorescence enhancement. The detection limits for Fe³⁺ and Cu²⁺ reached 8.1×10^{-8} M and 4.8×10^{-7} M, respectively. Furthermore, it was found that this probe can also be used for fluorescence imaging of Fe³⁺ and Cu²⁺ in living cells.

Keywords Rhodamine B · Colorimetric and fluorescent probe, cell imaging · Fe³⁺ · Cu²⁺

Introduction

Iron and copper are necessary trace elements for maintaining human normal function. For instance, iron is an essential component of hemoglobin that participate in oxygen delivery [1]. The deficiency of iron may lead to anemia, developmental retardation, apocleisis, and abalienation diseases [2–5]. Copper plays significant roles in iron absorption, enzymatic activity, tissue development and differentiation, and the function of central nervous system [6–8]. Copper deficiency is closely associated with indirect anemia, malnutrition, osteoporosis, neurodegenerative diseases [9–11]. However, superfluous iron and copper will generate potential cytotoxicity resulting in tissue and nerve damage [12–14]. For the normal organism, the amounts of both Fe³⁺ and Cu²⁺ ions maintain at a healthy level in tissues

and blood. Nevertheless, superfluous Fe³⁺ and Cu²⁺ will be released from iron-containing proteins when the body is diseased [15]. So investigations of Fe³⁺ and Cu²⁺ are of great significance to the early diagnosis of some diseases.

Optical analysis technique has proven to be a convenient tool for the detections of metal ions, anions, amino acids and proteins on account of its simple operation, excellent performance, fast and visualization [16–25]. At present, a lot of optical probes based on ultraviolet absorption and fluorescence have been reported and realized the detection of Fe³⁺ and Cu²⁺, successfully [26–35]. However, colorimetric and fluorescent probes for detection of Fe³⁺ and Cu²⁺ are quite limited [36–40]. Rhodamine B derives can complex with metal ions and occur ring-opening of the spirolactam, which result in color change and fluorescence enhancement [41–45]. On this basis, we synthesized a series of fluorescence probes based on rhodamine B and benzaldehyde derivatives. Among of them, probe 1 showed good recognition for Fe³⁺ and Cu²⁺ with turn on fluorescence, probe 2 and 3 displayed very good selectivity for Fe³⁺ and Cu²⁺ with significant fluorescence enhancement, respectively, while probe 4 and 5 exhibited poor selectivity because they exhibited enhanced fluorescence responses to multiple metal ions. This selectivity difference of different probes is mainly because the different substituents on the benzaldehyde groups change the binding ability between probe and metal ion. Herein we take probe 1 as an example to study the detection performance by ultraviolet absorption spectrum and fluorescence spectrum in detail.

Electronic supplementary material The online version of this article (<https://doi.org/10.1007/s10895-019-02438-5>) contains supplementary material, which is available to authorized users.

✉ Liqiang Yan
liqiangyan@glut.edu.cn

✉ Jianping Li
likianping@263.net

¹ Guangxi Colleges and Universities Key Laboratory of Food Safety and Detection, Guangxi Key Laboratory of Electrochemical and Magnetochemical Functional Materials, Guilin University of Technology, Guilin, Guangxi 541004, People's Republic of China

It was found that probe 1 can be used as optical probe to investigate Fe^{3+} and Cu^{2+} with different color changes and different emission wavelengths.

Experimental

Materials and Equipment

^1H NMR and ^{13}C NMR spectra were measured using a nuclear magnetic resonance spectrometer (AVANCE III HD 600 MHz, Bruker, Switzerland), UV-visible absorption spectra and fluorescence spectra were gathered by UV-vis spectrometer (Lambda 950, PerkinElmer, USA) and Cary Eclipse fluorescence spectrophotometer (Varian, America), respectively. Fluorescence images were taken using laser scanning confocal microscopy (LSM700, Zeiss, Germany).

Rhodamine B (98%), benzaldehyde derivatives (AR), solvents (AR) and cationic nitrates were purchased from Aladdin reagent (Shanghai) co. LTD (China) and used directly without treatment. Redistilled water was used to prepare water solution.

Absorbance and Fluorescence Spectra

Stock solutions of probe (10 nM) and metal ions (100 nM) were prepared in the mixture of CH_3CN and HEPES solution (1:1, v:v, pH 7.4) and were further adjusted their concentrations by the addition of the mixture solution of CH_3CN and HEPES solution (1:1, v:v, pH 7.4) for testing purposes. Excitation was set at 555 nm with excitation and emission slit widths at 5 nm.

Laser Confocal Imaging

Human non-small cell lung cancer A549 cells were purchased Shanghai Chaoyan Biotechnology Co., Ltd. And they were grown in Dulbecco's modified eagle medium (DMEM) culture at 37 °C with 5% CO_2 in a 12 well cell culture plate. Two groups of A549 cells were cultured with probe 1 (20 μM) for 20 min and then incubated respectively with Fe^{3+} (20 μM) and Cu^{2+} (20 μM). Washed three times with PBS, confocal imaging was carried out upon emission window of red channel and 20 \times objective lens. Laser wavelength and detection wavelength were 561 nm and 570–670 nm, respectively.

Synthesis of Probe 1–5

Probe 1–5 were synthesized using similar method (Scheme S1). Briefly, 4 mL of hydrazine hydrate (85%) was added dropwise into the mixture of rhodamine B (2.4 g, 5 mmol) and anhydrous $\text{C}_2\text{H}_5\text{OH}$ (50 mL) solution with vigorous stirring. The solution was refluxed for 2 h, cooled and removed

solvent under reduced pressure. The resulting solid was dissolved again in 100 mL of HCl (1 M) and adjusted pH to 9–10 using NaOH (1 M). Rhodamine B hydrazide (yield, 75%) was got after filtered and washed three times with water. Then Rhodamine B hydrazide reacted with benzaldehyde derivatives with 1:1 of molar ratio in anhydrous $\text{C}_2\text{H}_5\text{OH}$ (20 mL) under reflux condition. The target products were collected by the suction filtration (Scheme 1).

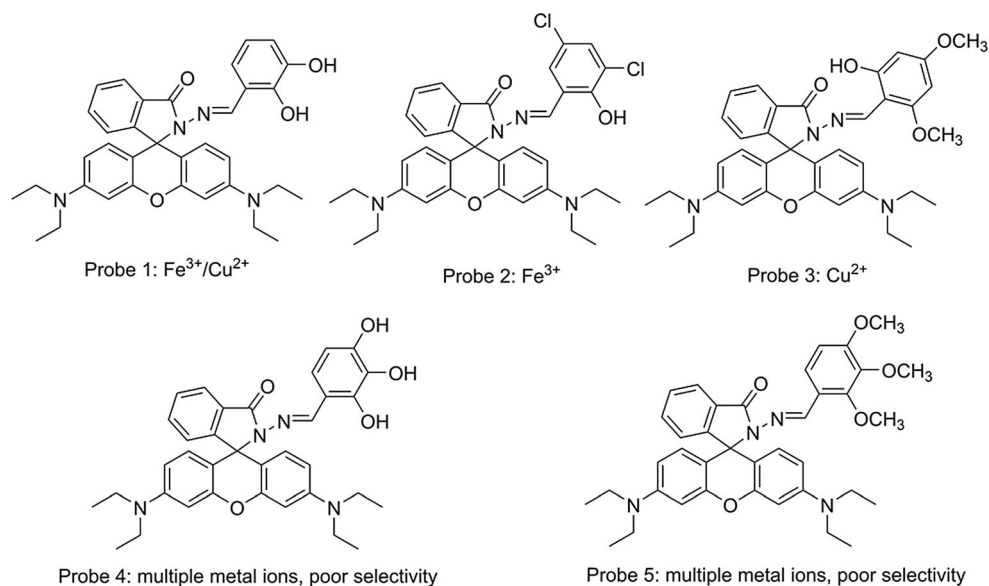
Probe 1, pink solid, Yield, 71.2%, ^1H NMR (CDCl_3 , 600 MHz): δ (ppm): 11.14 (s, 1H); 9.03 (s, 1H); 7.99–7.98 (d, 1H, $J=6$ Hz); 7.55–7.51 (m, 2H); 7.17–7.16 (d, 1H, $J=6$ Hz); 6.86–6.85 (d, 1H, $J=6$ Hz); 6.70–6.67 (m, 2H); 6.50–6.49 (d, 1H, $J=6$ Hz); 6.46–6.45 (d, 2H, $J=6$ Hz); 6.28–6.26 (d, 2H, $J=12$ Hz); 5.67 (s, 1H); 3.35–3.31 (q, 8H, $J=6$ Hz); 1.17–1.15 (t, 12H, $J=6$ Hz). ^{13}C NMR (CDCl_3 , 151 MHz): 164.3, 153.4, 151.2, 151.1, 149.1, 145.3, 144.8, 133.6, 128.6, 128.2, 124.1, 123.4, 122.3, 119.2, 116.1, 108.3, 105.1, 97.9, 66.3, 44.4, 12.6. EI-MS calcd for $\text{C}_{35}\text{H}_{36}\text{N}_4\text{O}_4$ 577.27, found 577.28 [$\text{M} + \text{H}$] $^+$.

Probe 2, brown solid, Yield, 71.2%, ^1H NMR (CDCl_3 , 600 MHz): δ (ppm): 11.55 (s, 1H); 8.78 (s, 1H); 7.99–7.98 (d, 1H, $J=6$ Hz); 7.55–7.49 (m, 2H); 7.24 (s, 1H); 7.15–7.14 (d, 1H, $J=6$ Hz); 6.94 (s, 1H); 6.49–6.47 (m, 4H); 6.27–6.25 (m, 2H); 3.35–3.31 (q, 8H, $J=6$ Hz); 1.17–1.15 (t, 12H, $J=6$ Hz). ^{13}C NMR (CDCl_3 , 151 MHz): 164.6, 153.2, 152.9, 151.5, 149.2, 148.5, 134.0, 130.6, 128.9, 128.7, 128.0, 124.1, 123.6, 122.3, 120.3, 106.1, 104.6, 98.0, 66.2, 44.4, 12.6. EI-MS calcd for $\text{C}_{35}\text{H}_{34}\text{Cl}_2\text{N}_4\text{O}_3$ 628.20, found 629.21 [$\text{M} + \text{H}$] $^+$.

Probe 3, brown solid, Yield, 63.1%, ^1H NMR (CDCl_3 , 600 MHz): δ (ppm): 11.54 (s, 1H); 9.54 (s, 1H); 7.96–7.95 (d, 1H, $J=6$ Hz); 7.51–7.49 (m, 2H); 7.17–7.16 (d, 1H, $J=6$ Hz); 6.50–6.45 (m, 4H); 6.26–6.25 (d, 2H, $J=6$ Hz); 5.86–5.85 (d, 1H, $J=6$ Hz); 3.72–3.71 (d, 6H, $J=6$ Hz); 3.33–3.30 (q, 8H, $J=6$ Hz); 1.16–1.13 (t, 12H, $J=6$ Hz). ^{13}C NMR (CDCl_3 , 151 MHz): 163.6, 163.3, 161.8, 160.1, 153.7, 150.8, 150.7, 148.9, 133.1, 130.6, 128.5, 128.3, 124.1, 123.1, 108.0, 105.6, 102.0, 97.9, 93.4, 90.2, 66.4, 44.4, 12.6. EI-MS calcd for $\text{C}_{37}\text{H}_{40}\text{N}_4\text{O}_5$ 620.30, found 621.32 [$\text{M} + \text{H}$] $^+$.

Probe 4, brown solid, Yield, 61.5%, ^1H NMR (CDCl_3 , 600 MHz): δ (ppm): 11.29 (s, 1H); 9.0 (s, 1H); 7.98–7.97 (d, 1H, $J=6$ Hz); 7.54–7.49 (m, 2H); 7.16–7.15 (d, 1H, $J=6$ Hz); 6.62–6.60 (d, 1H, $J=12$ Hz); 6.50–6.49 (d, 2H, $J=6$ Hz); 6.45–6.42 (m, 3H); 6.28–6.26 (m, 2H); 5.61 (s, 1H); 5.52 (s, 1H); 3.35–3.31 (q, 8H, $J=6$ Hz); 1.17–1.15 (t, 12H, $J=6$ Hz). ^{13}C NMR (CDCl_3 , 151 MHz): 164.1, 153.4, 152.6, 149.0, 146.1, 133.4, 131.1, 128.5, 128.2, 124.0, 123.3, 123.1, 112.1, 108.2, 106.8, 105.2, 97.8, 66.2, 44.4, 12.6. EI-MS calcd for $\text{C}_{35}\text{H}_{36}\text{N}_4\text{O}_5$ 592.27, found 593.26 [$\text{M} + \text{H}$] $^+$.

Probe 5, brown solid, Yield, 48.2%, ^1H NMR (CDCl_3 , 600 MHz): δ (ppm): 8.85 (s, 1H); 8.00–7.99 (d, 1H, $J=6$ Hz); 7.51–7.46 (m, 2H); 7.40 (s, 1H); 7.14–7.13 (d, 1H, $J=6$ Hz); 6.53–6.51 (d, 2H, $J=12$ Hz); 6.41 (s, 2H); 6.35 (s, 1H); 6.24–6.23 ((d, 2H, $J=6$ Hz); 3.86–3.84 (d, 6H, $J=12$ Hz); 3.36 (s, 3H); 3.33–3.30 (q, 8H, $J=6$ Hz); 1.15–1.12 (t,

Scheme 1 Structures of probes 1–5

12H, $J = 6$ Hz). ^{13}C NMR (CDCl_3 , 151 MHz): 164.5, 153.7, 153.3, 151.5, 151.4, 148.8, 143.6, 143.1, 133.1, 129.9, 128.3, 128.1, 123.9, 123.2, 116.5, 107.9, 107.8, 106.2, 97.7, 97.7, 66.0, 57.4, 56.1, 56.0, 44.3, 12.6. EI-MS calcd for $\text{C}_{38}\text{H}_{42}\text{N}_4\text{O}_5$ 634.32, found 635.32 $[\text{M} + \text{H}]^+$.

Discussion and Results

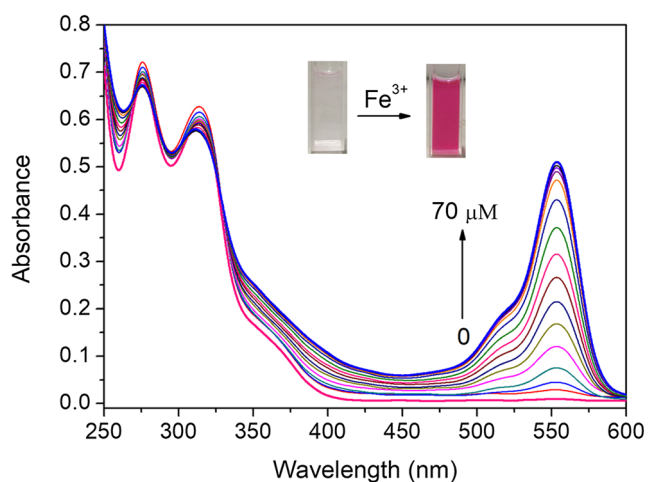
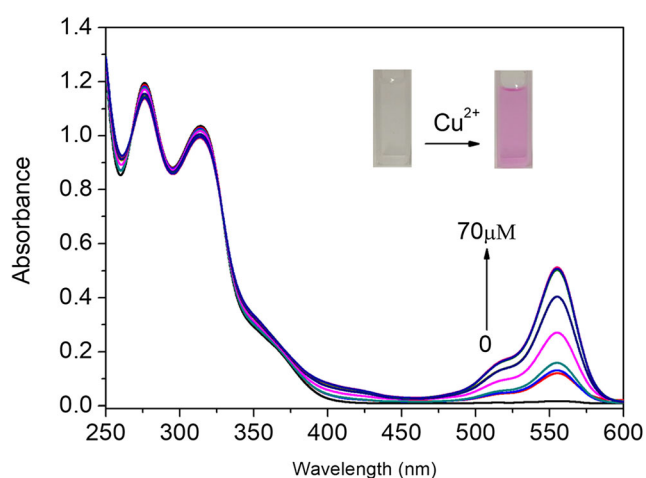
Absorption Spectra

The absorption responses of probe 1 to Fe^{3+} and Cu^{2+} were firstly investigated. As shown in Fig. 1, probe 1 solution has three absorbance peaks at 275 nm, 314 nm and 554 nm. When a series of concentrations of Fe^{3+} (0, 5, 10, 15, 20, 25, 30, 35, 40, 45, 50, 55, 60, 65, 70 μM) were added into probe 1 solution, a new absorbance peak at 554 nm came out and

improved gradually to a stable value. While the peaks at 275 nm and 314 nm gradually decreased. The color of probe 1 solution changed from colorless to amaranth accordingly, which could be recognized easily by naked eye (Fig. 1 inset). Probe 1 showed a similar trend along with the gradual addition of Cu^{2+} (0, 5, 10, 15, 20, 25, 30, 35, 40, 45, 50, 55, 60, 65, 70 μM). As shown in Fig. 2, the absorbance peaks at 555 nm increased step by step, while the peaks at 275 nm and 314 nm weakened gradually. The color of probe 1 changed from colorless to pink (Fig. 2 inset). It can be concluded that probe 1 can realized visual detection by colorimetric method.

Fluorescence Response

The sensitivities of probe 1 for the detection of Fe^{3+} and Cu^{2+} were further examined. As shown in Fig. 3, the fluorescence intensity of probe 1 (10 μM) enhanced gradually

**Fig. 1** Absorbance spectra of probe 1 along with addition of a series of Fe^{3+} (0–70 μM)**Fig. 2** Absorbance spectra of probe 1 along with addition of a series of Cu^{2+} (0–70 μM)

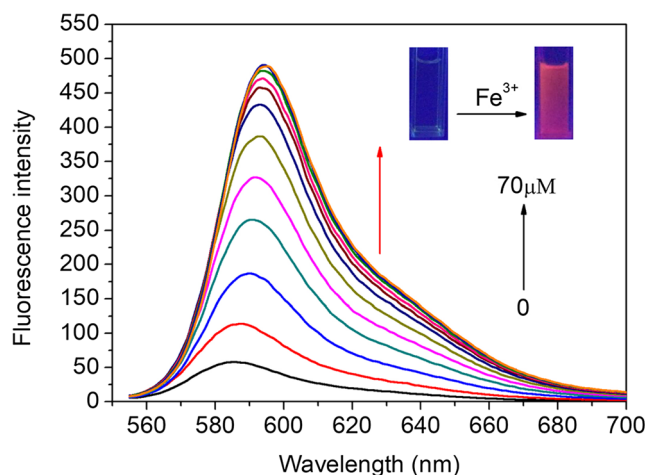


Fig. 3 Fluorescence spectra of probe 1 (10 μM) along with addition of a series of Fe^{3+} (0–70 μM)

and the fluorescence peak red shifted slowly to 595 nm from 585 nm along with the concentration increase of Fe^{3+} from 0 to 70 μM . Similarly, the fluorescence of probe 1 increased gradually and the emission peak blue shifted to 575 nm from 585 nm when a variety of Cu^{2+} (0, 5, 10, 15, 20, 25, 30, 35, 40, 45, 50, 55, 60, 65, 70 μM) were added to probe 1 solution (Fig. 4). Meanwhile, it can be found from Fig. 5 that the fluorescence intensity of probe 1 has linear relation to the concentration of Fe^{3+} from 0 to 35 μM , and the linear equation is $y = 50.4 + 13.0x$ ($R^2 = 0.9957$), which can be used for the quantitative analysis of Fe^{3+} . And the linear equation between fluorescence intensity of probe 1 and the concentration of Cu^{2+} was also found as $y = 50.4 + 2.2x$ ($R^2 = 0.9718$) when the concentration is within the range of 0–45 μM . The limit of detection (LOD) of probe 1 to Fe^{3+} could be calculated as 8.1×10^{-8} M when SNR (signal to noise ratio) is 3 and RSD (relative standard deviation) is

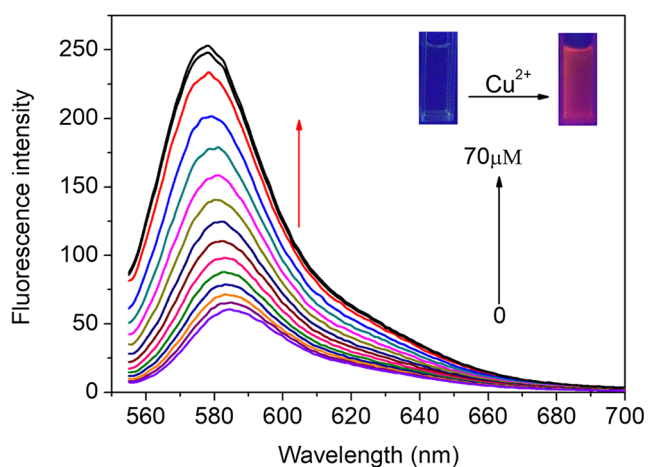


Fig. 4 Fluorescence spectra of probe 1 (10 μM) along with addition of a series of Cu^{2+} (0–70 μM)

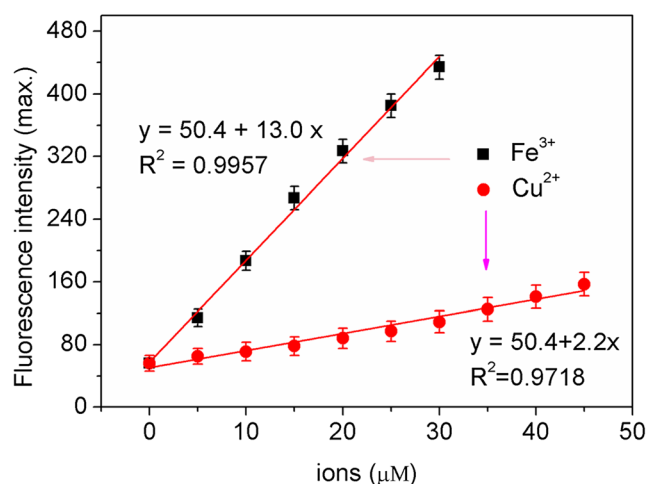


Fig. 5 The linear relations between the fluorescence intensities of probe 1 and the concentrations of Fe^{3+} (black square) and Cu^{2+} (red dot)

3.5% according to the literature calculation method [46]. In the same way, the LOD of probe 1 to Cu^{2+} is 4.8×10^{-7} M. The results indicates probe 1 has high sensitivity to Fe^{3+} and Cu^{2+} .

In addition, the selectivity and anti-interference ability are exhibited in Fig. 6. After addition of Fe^{3+} (70 μM) and Cu^{2+} (70 μM), the fluorescence intensity of probe 1 (10 μM) solution showed significant enhancement. While other common metal ions (70 μM) including Na^+ , K^+ , Li^+ , Ag^+ , Pb^{2+} , Cd^{2+} , Co^{2+} , Ni^{2+} , Ba^{2+} , Ca^{2+} , Mg^{2+} , Zn^{2+} , Fe^{2+} , Al^{3+} , Cr^{3+} , did not bring about significant changes in fluorescence of probe 1 (blue bars). The results indicated that probe 1 has excellent selectivity for Fe^{3+} and Cu^{2+} . In addition, this selectivity was not disturbed by other metal ions. When interfering ions were added respectively into the solutions of probe 1 in the presence

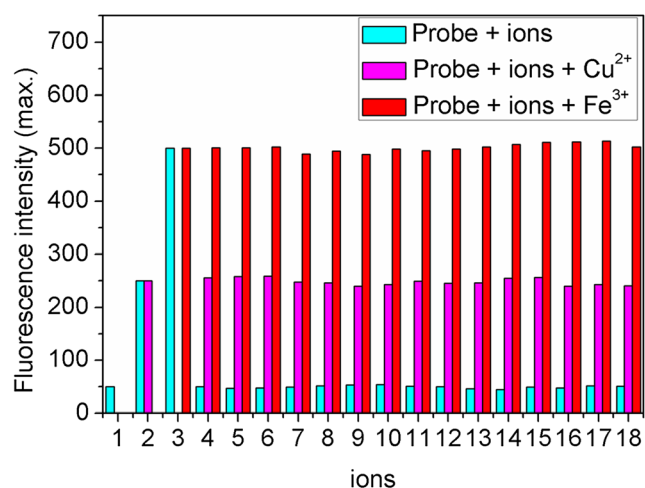


Fig. 6 Fluorescence intensities of probe 1 (blue bar) and its complexes with Fe^{3+} (red bar) and Cu^{2+} (violet bar) in the presence of various metal ions. 1: probe 1, 2: Cu^{2+} , 3: Fe^{3+} , 4: Na^+ , 5: K^+ , 6: Li^+ , 7: Ag^+ , 8: Pb^{2+} , 9: Cd^{2+} , 10: Co^{2+} , 11: Ni^{2+} , 12: Ba^{2+} , 13: Ca^{2+} , 14: Mg^{2+} , 15: Zn^{2+} , 16: Fe^{2+} , 17: Al^{3+} , 18: Cr^{3+}

of Fe^{3+} (Fig. 6 red bars), no significant decrease of the fluorescence maximum values was observed. These interfering ions also did cause noteworthy decrease in fluorescence of probe 1 with Cu^{2+} (violet bars). Therefore, probe 1 has excellent selectivity and anti-interference ability.

The fluorescence detection for metal ions is dependent greatly on the test condition. Hence, the fluorescence change of probe 1 in the presence of Cu^{2+} and Fe^{3+} over response time and pH were tested. As displayed in Fig. 7, the fluorescence of probe 1 reached the maximum quickly in 10 min after addition of Cu^{2+} and Fe^{3+} under stirring. In addition, the fluorescence intensities of probe 1 and probe 1 with Cu^{2+} improved observably when pH is less than 4, which may be because H^+ binds to the amino group of probe and causes the ring-opening of the spirolactam under acidic condition. While the fluorescence intensities of probe 1 with Cu^{2+} and Fe^{3+} decreased sharply when pH is more than 8, which is mainly because the complex of OH^- and metal ions hinders the interaction between metal ions and probe molecules. As a result, the best pH values should be between 4 and 8 (Fig. 8).

Application of Probe in Fluorescence Image in Live Cells

Probe 1 was applied to fluorescence image in live A549 cells. No fluorescence was observed when A549 cells were incubated with probe 1 (20 μM) for 20 min (Fig. S12 b, e). However there were strong red fluorescence when A549 cells were treated with probe 1 (20 μM) for 20 min and then cultured with 20 μM of Cu^{2+} (Fig. S12 c) and Fe^{3+} (Fig. S12 g) for 10 min, respectively. And the images in bright field (Fig. S12 a, e) indicated that the cells were living. Thus, probe 1 provides fluorescence Off-On images for the cellular Fe^{3+} and Cu^{2+} ions.

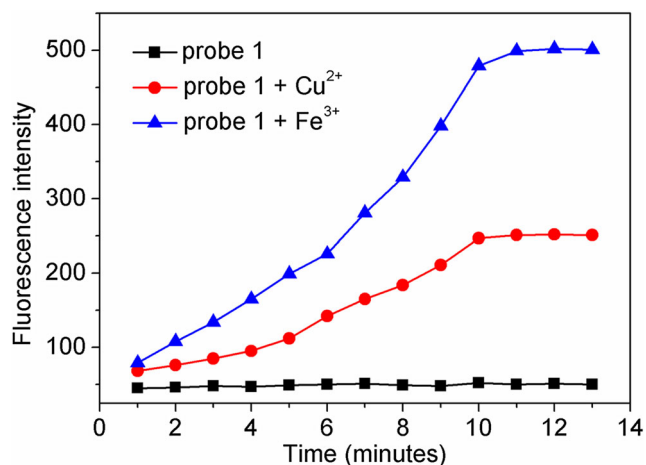


Fig. 7 Fluorescence intensity change of probe 1 over time (1–13 min) after addition of Cu^{2+} (70 μM) and Fe^{3+} (70 μM)

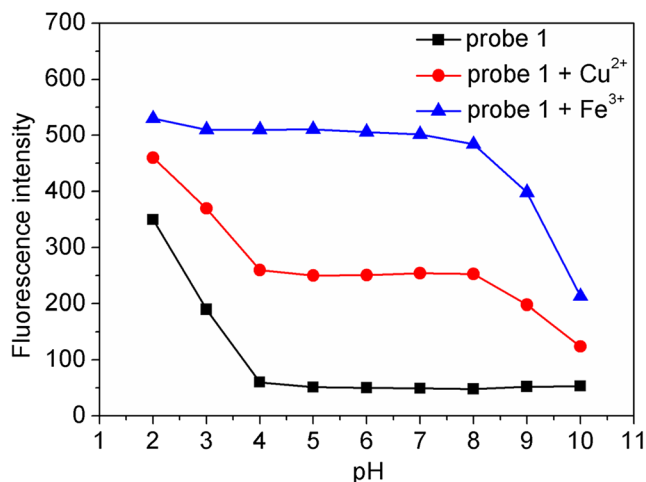


Fig. 8 Maximum fluorescence intensity of probe 1 (10 μM) and in the presence of Cu^{2+} (70 μM) and Fe^{3+} (70 μM) with different pH conditions

Conclusions

In brief, we developed a rhodamine B-based optical probe (probe 1) and investigated its colorimetric and fluorescence responses to Fe^{3+} and Cu^{2+} . Probe 1 showed remarkable color changes from colorless to amaranth and to pink after addition of Fe^{3+} and Cu^{2+} , respectively. Moreover, along with the addition of Fe^{3+} and Cu^{2+} , its fluorescence wavelengths red shifted 595 nm and blue shifted to 575 nm from 585 nm, respectively, which can draw a distinction between Fe^{3+} and Cu^{2+} . Additionally, probe 1 exhibited excellent fluorescence image ability in living cells by laser confocal microscopy. Therefore, this probe can be used to the qualitative and quantitative test, and intracellular fluorescence analysis.

Acknowledgments This work was supported by Natural Science Foundation of Guangxi Province (2018GXNSFBA281070, 2015GXNSFFA139005), Foundation of Guilin University of Technology (GUTQDJJ2017), and High Level Innovation Teams of Guangxi Colleges and Universities and Outstanding Scholars Program (Guijiaoren [2014]49).

References

- Ganz T (2007) Molecular control of iron transport. *J Am Nephrol* 18:394–400
- Beutler E, Felitti V, Gelbart T, Ho N (2001) Genetics of iron storage and hemochromatosis. *Drug Metab Dispos* 29:495–499
- Ong WY, Farooqui AA (2005) Iron, neuroinflammation, and Alzheimer's disease. *J Alzheimers Dis* 8:183–200
- Fleming RE, Ponka P (2012) Iron overload in human disease. *N Engl J Med* 366:348–359
- Luo A, Wang H, Wang Y, Huang Q, Zhang Q (2016) A novel colorimetric and turn-on fluorescent chemosensor for iron(III) ion detection and its application to cellular imaging. *Spectrochim Acta A* 168:37–44
- Bibudhendra S (1999) Treatment of Wilson and menkes diseases. *Chem Rev* 99:2535–2544

7. Gaggell E, Kozlowski H, Valensin D, Valensin G (2006) Copper homeostasis and neurodegenerative disorders (alzheimer's, prion, and parkinson's diseases and amyotrophic lateral sclerosis). *Chem Rev* 106:1995–2044
8. Kalinowski DS, Richardson DR (2007) Future of Toxicology/Iron chelators and differing modes of action and toxicity: the changing face of Iron chelation therapy. *Chem Res Toxicol* 20:715–720
9. Barnham KJ, Masters CL, Bush AI (2004) Neurodegenerative diseases and oxidative stress. *Nat Rev Drug Discov* 3:205–214
10. Stern BR, Solioz M, Krewski D, Aggett P, Aw TC, Baker S, Crump K, Dourson M, Haber L, Hertzberg R, Keen C, Meek B, Rudenko L, Schoeny R, Slob W, Starr T (2007) Copper and human health: biochemistry, genetics, and strategies for modeling dose-response relationships. *J Toxicol Env Heal B* 10:157–222
11. Uauy R, Olivares M, Gonzalez M (1998) Essentiality of copper in humans. *Am J Clin Nutr* 67:952S–959S
12. Swaminathan S, Fonseca VA, Alam MG, Shah SV (2007) The role of iron in diabetes and its complications. *Diabetes Care* 30:1926–1933
13. Halliwell B (1992) Reactive oxygen species and the central nervous system. *J Neurochem* 59:1609–1623
14. Galaris D, Skiada V, Barbouti A (2008) Redox signaling and cancer: the role of “labile” iron. *Cancer Lett* 266:21–29
15. Zecca L, Youdim MB, Riederer P, Connor JR, Crichton RR (2004) Iron, brain aging and neurodegenerative disorders. *Nat Rev Neurosci* 5:863–873
16. Yan L, Li X, Li J (2018) A novel turn-on fluorescent probe based on coumarin schiff's base for multichannel monitoring of Al^{3+} , Hg^{2+} and ClO^- in different solutions and its applications. *ChemistrySelect* 3:10157–10163
17. Yan L, Hu C, Li J (2018) A fluorescence turn-on probe for rapid monitoring of hypochlorite based on coumarin Schiff base. *Anal Bioanal Chem* 410:7457–7464
18. Hu C, Li J, Yan L (2019) A fluorescent probe for hypochlorite with colorimetric and fluorometric characteristics and imaging in living cells. *Anal Biochem* 566:32–36
19. Yan L, Nan D, Lin C, Wan Y, Pan Q, Qi Z (2018) A near-infrared fluorescent probe for rapid detection of carbon monoxide in living cells. *Spectrochim Acta A* 202:284–289
20. Du J, Ma W, Gu Q, Yao Q, Long S, Sun W, Fan J, Peng X (2019) Thiol-activated fluorescent probe for sensitive detection and imaging of proteins. *Sensors Actuators B Chem* 287:118–123
21. Xie Y, Yan L, Tang Y, Tang M, Wang S, Bi L, Sun W, Li J (2019) A smart fluorescent probe based on salicylaldehyde schiff's base with AIE and ESIPT characteristics for the detections of N_2H_4 and ClO^- . *J Fluoresc* 29:399–406
22. Noom MC, Van Den Broek B, Van Mameren J, Wuite GJ (2007) Visualizing single DNA-bound proteins using DNA as a scanning probe. *Nat Methods* 4:1031–1036
23. Okada T, Yamamoto Y, Miyachi H, Karube I, Muramatsu H (2007) Application of peptide probe for evaluating affinity properties of proteins using quartz crystal microbalance. *Biosens Bioelectron* 22:1480–1486
24. Zhang H, Liu R, Tan Y, Xie WH, Lei H, Cheung HY, Sun H (2015) A FRET-based ratiometric fluorescent probe for nitroxyl detection in living cells. *ACS Appl Mater Interfaces* 7:5438–5443
25. Li R, Chai X, Cui X, Jiang Y, Zhang D, Wang T (2018) A fluorescence resonance energy transfer based pH probe for visualizing acidification in fungal cells. *Sensors Actuators B Chem* 274:533–540
26. Tang T, Guo W, Zhang Y, Xu D (2019) A novel 1, 8-naphthalimide-based “turn-on” fluorescent sensor for Fe^{3+} . *J Fluoresc* 29:445–450
27. Yan L, Gu X, Wang Z, Qi Z (2018) Fe^{3+} -responsive micelle based on an amphiphilic polymer and a rhodamine B-containing amphiphile in aqueous media. *ChemistrySelect* 3:3406–3410
28. Cao X, Zhang F, Bai Y, Ding X, Sun W (2019) A highly selective “turn-on” fluorescent probe for detection of Fe^{3+} in cells. *J Fluoresc* 29:425–434
29. Zhang Z, Li F, He C, Ma H, Feng Y, Zhang Y, Zhang M (2018) Novel Fe^{3+} fluorescence probe based on the charge-transfer (CT) molecules. *Sensors Actuators B Chem* 255:1878–1883
30. Jin X, Gao J, Xie P, Yu M, Wang T, Zhou H, Ma A, Wang Q, Leng X, Zhang X (2018) Dual-functional probe based on rhodamine for sequential Cu^{2+} and ATP detection in vivo. *Spectrochim Acta A* 204:657–664
31. Zheng X, Ji R, Cao X, Ge Y (2017) FRET-based ratiometric fluorescent probe for Cu^{2+} with a new indolizine fluorophore. *Anal Chim Acta* 978:48–54
32. Fang H, Huang PC, Wu FY (2019) A highly sensitive fluorescent probe with different responses to Cu^{2+} and Zn^{2+} . *Spectrochim Acta A* 214:233–238
33. Zhao C, Chen J, Cao D, Wang J, Ma W (2019) Novel coumarin-based containing denrons selective fluorescent chemosensor for sequential recognition of Cu^{2+} and PPI. *Tetrahedron* 75:1997–2003
34. Park Y, Lee CY, Park KS, Park HG (2017) Enzyme-free colorimetric detection of Cu^{2+} by utilizing target-triggered DNAzymes and toehold-mediated DNA strand displacement events. *Chem Eur J* 23:17379–17383
35. Chen F, Xiao F, Zhang W, Lin C, Wu Y (2018) Highly stable and NIR luminescent Ru-LPMSN hybrid materials for sensitive detection of Cu^{2+} in vivo. *ACS Appl Mater Interfaces* 10:26964–26971
36. Li N-N, Ma Y-Q, Sun X-J, Li M-Q, Zeng S, Xing Z-Y, Li J-L (2019) A dual-function probe based on naphthalene for fluorescent turn-on recognition of Cu^{2+} and colorimetric detection of Fe^{3+} in neat H_2O . *Spectrochim Acta A* 210:266–274
37. Bhorge YR, Tsai H-T, Huang K-F, Pape AJ, Janaki SN, Yen Y-P (2014) A new pyrene-based Schiff-base: a selective colorimetric and fluorescent chemosensor for detection of Cu(II) and Fe(III). *Spectrochim Acta A* 130:7–12
38. Zhang M, Gong L, Sun C, Li W, Chang Z, Qi D (2019) A new fluorescent-colorimetric chemosensor based on a Schiff base for detecting Cr^{3+} , Cu^{2+} , Fe^{3+} and Al^{3+} ions. *Spectrochim Acta A* 214:7–13
39. Roy N, Dutta A, Mondal P, Paul PC, Singh TS (2017) Coumarin based fluorescent probe for colorimetric detection of Fe^{3+} and fluorescence turn on-off response of Zn^{2+} and Cu^{2+} . *J Fluoresc* 27:1307–1321
40. Yang Y, Yu K, Yang L, Liu J, Li K, Luo S (2015) One single molecule as a multifunctional fluorescent probe for ratiometric sensing of Fe^{3+} , Cr^{3+} and colorimetric sensing of Cu^{2+} . *Sensors* 15:49–58
41. Hu J, Hu Z, Chen Z, Gao HW, Uvdal K (2016) A logic gate-based fluorogenic probe for Hg^{2+} detection and its applications in cellular imaging. *Anal Chim Acta* 919:85–93
42. Chen XQ, Pradhan T, Wang F, Kim JS, Yoon J (2012) Fluorescent chemosensors based on spiroring-opening of xanthenes and related derivatives. *Chem Rev* 112:1910–1956
43. Gao Z, Kan C, Liu H, Zhu J, Bao X (2019) A highly sensitive and selective fluorescent probe for Fe^{3+} containing two rhodamine B and thiocarbonyl moieties and its application to live cell imaging. *Tetrahedron* 75:1223–1230
44. Lv T, Xu Y, Li H, Liu F, Sun S (2018) A rhodamine B-based fluorescent probe for imaging Cu^{2+} in maize roots. *Bioorgan Med Chem* 26:1448–1452
45. Pang BJ, Li CR, Yang ZY (2018) A novel chromone and rhodamine derivative as fluorescent probe for the detection of Zn (II) and Al (III) based on two different mechanisms. *Spectrochim Acta A* 204:641–647
46. Yan L, Li R, Ma F, Qi Z (2017) A simple salicylaldehyde-based fluorescent “turn-on” probe for selective detection of Zn^{2+} in water solution and its application in live cell imaging. *Anal Methods* 9:1119–1124

Publisher's Note Springer Nature remains neutral with regard to jurisdictional claims in published maps and institutional affiliations.